

Combined Application of Dentin Noncollagenous Proteins and Odontogenic Biphasic Calcium Phosphate in Rabbit Maxillary Sinus Lifting

Gang Yang¹ · Xin Liu² · Tianyu Huang¹ · Ruyuan Ding¹ · Yuanyin Wang¹ 

Received: 22 June 2022 / Revised: 17 October 2022 / Accepted: 25 October 2022 / Published online: 24 December 2022
© Korean Tissue Engineering and Regenerative Medicine Society 2022

Abstract

BACKGROUND: Teeth can be used as a raw material for preparing bone substitutes due to their similar chemical composition to bone. The objective of our study was to evaluate the effect of odontogenic biphasic calcium phosphate (BCP) incorporating dentin noncollagenous proteins (DNCPs) on osteogenesis and stability in maxillary sinus augmentation.

METHODS: The composition, structure and morphology of the odontogenic BCP were tested by X-ray powder diffraction (XRD), Brunauer–Emmett–Teller, and scanning electron microscopy methods. The biocompatibility and osteoinduction of DNCPs and materials were examined *in vitro* and their bone regeneration capacity was verified *in vivo*.

RESULTS: The results showed that the cells adhered and proliferated well on the DNCP-loaded BCP scaffold. The odontogenic BCP and DNCPs promoted osteogenic differentiation of cells, The new bone formation in the BCP groups and DNCP subgroups was significantly higher than the new bone formation in the control, and the new bone quality was better. The bone regeneration effect of odontogenic BCP was similar to the effect of deproteinized bovine bone mineral, but β -TCP did not maintain the height and volume of bone reconstruction.

CONCLUSION: In conclusion, the combined application of DNCPs and odontogenic BCP is an effective strategy for tissue engineering osteogenesis in the maxillary sinus region. The biomimetic strategy could provide a new approach for patients requiring maxillary sinus lifting.

Keywords Dentin noncollagenous proteins · Biphasic calcium phosphate · Tissue engineering osteogenesis · Maxillary sinus lifting

Gang Yang and Xin Liu contributed equally to this work and should be considered co-first authors.

✉ Xin Liu
xindyliu@126.com

✉ Yuanyin Wang
wyy1970548@sohu.com

¹ Key Laboratory of Oral Diseases Research of Anhui Province, Oral and Maxillofacial Surgery, Stomatologic Hospital & College, Anhui Medical University, 81 Meishan Road, Hefei 230032, Anhui, China

² Key Laboratory of Oral Diseases Research of Anhui Province, Department of Oral Implant, Oral and Maxillofacial Center, Stomatologic Hospital & College, Anhui Medical University, 81 Meishan Road, Hefei 230032, Anhui, China

1 Introduction

With the development of dental implant restoration, increasing attention has been given to the treatment of complex cases with insufficient vertical bone height in the maxillary region and maxillary sinus elevation is an effective method to improve vertical bone height [1–3]. In the clinic, we often implant bone substitute material between the maxillary sinus floor and membrane to increase bone mass. However, the maxillary sinus is a special environment, and the sinus cavity is an air cavity that exerts a certain pressure on the surrounding area with respiratory movement. To achieve good bone reconstruction, simulating the composition and structure of bone

tissue has been spotlighted as an approach to tissue engineering technology [4, 5]. Calcium phosphate ceramics have a chemical composition similar to bone and have been widely used as bone scaffolds. The most commonly used calcium phosphate ceramics are hydroxyapatite (HA) and β -tricalcium phosphate (β -TCP) [6, 7]. However, in the process of repairing bone defects, the degradation rate of β -TCP does not match the growth rate of new bone, which is not conducive to osteogenesis [8, 9]. HA can bind directly with bone tissue, but the degradation rate is far less than the degradation rate of β -TCP [10, 11].

Biphasic calcium phosphate (BCP) has the presence and uniform distribution of HA and β -TCP in the same particle. Calcium phosphate bioceramic is a promising material for bone repair due to its excellent properties. Among them, BCP materials have been widely used and studied [12–14]. Straumann® Bone Ceramic was used as a BCP bone substitute in maxillary sinus lifting and achieved good results, allowing dental implants after the six-month healing period [15]. BCP with different HA/ β -TCP ratios (e.g., 70:30, 60:40, 30:70, 20:80) was reported to have excellent effects as a bone graft material [16–18]. The differences in preparation method and raw material will affect its porosity, pore size, particle size, surface morphology and other structures and properties, all of which will affect its osteogenic ability [19–22]. Bone tissue is a highly mineralized hard tissue that is formed mainly by the interaction of collagen fiber and hydroxyapatite in a certain arrangement. Mineralization of the bone matrix is a key factor in determining the bone quality and mechanical properties, and near the mineralization front, there are also noncollagen proteins (NCPs), although in small quantities, but several studies believe that the biomineralization process of bone tissue will be influenced by NCPs [23–26].

Previous studies have shown that bioactive material was obtained by calcination of animal bones [27]. Human teeth have a chemical composition similar to bone tissue and are a potential bone replacement material. Kim used the material acquired after tooth sintering to repair bone defects and observed new bone formation [28]. In terms of growth factors, the extracellular matrix (ECM) proteins of dentin and bone are similar in many aspects; they all express bone morphogenetic protein (BMP), dentin matrix protein (DMP 1), transforming growth factor beta (TGF- β), vascular endothelial growth factors (VEGFs), dentin sialophosphoprotein (DSPP), osteopontin (OPN), etc. [29, 30]. The molecular weight of these dentin noncollagenous proteins is mainly between 10 and 300 kDa [30, 31]. Previous studies have suggested that BMP-2 as growth factors promote osteogenic differentiation of bone marrow mesenchymal stem cells (BMSCs) *in vitro* or enhance bone regeneration *in vivo* [32, 33]. In addition, Sun et al. indicated that nanofibrous gelatin scaffolds with

NCPs induced bone tissue regeneration in skull defects [34].

In this study, we intended to completely apply extracted teeth as raw materials, partly extract dentin noncollagen proteins (DNCPs) as compound growth factors, partly obtain odontogenic BCP through sintering, and then examine the effectiveness of BCP incorporating DNCPs on bone tissue regeneration in the maxillary sinus area in rabbits. Deproteinized bovine bone mineral (DBBM, Bio-Oss®, Geistlich, Wolhusen, Switzerland) and β -TCP bone substitutes commonly applied clinically were used as control groups. The study can provide a new idea and method of tissue engineering osteogenesis for patients with bone insufficiency in the maxillary posterior region in dental implantation.

2 Materials and methods

2.1 Extraction of DNCPs

DNCPs were extracted from waste extracted teeth as previously described [34, 35]. The extracted healthy human teeth were collected from the oral and maxillofacial surgery department at stomatological hospital and stored at $-70\text{ }^{\circ}\text{C}$. Enamel, cementum, and pulp were removed, and then the teeth were crushed into small pieces with a surgical hammer and further prepared into powders. The dentin powders were placed in a mixture buffer of 4 M guanidine hydrochloride (Gdm-HCl) with protease inhibitors (0.78 mg/mL benzamide hydrochloride, 0.18 mg/mL sodium iodoacetate, 1.8 $\mu\text{g}/\text{mL}$ trypsin inhibitor, 5 $\mu\text{g}/\text{mL}$ pepstatin, and 5 mmol/L phenylmethylsulfonyl fluoride) for 48 h to extract NCPs that were present in the unmineralized predentin and osteoid. Then, a 0.5 M ethylenediaminetetraacetic acid (EDTA) solution with these protease inhibitors was added for more than 48 h to facilitate the release of proteins in the mineral matrix. Subsequently, a 4 M Gdm-HCl solution with protease inhibitors was used to again extract NCPs in the remaining demineralized dentin. The extract was centrifuged at 10,000 r for 30 min. The protein solution was placed in an 8-kDa dialysis tube and dialyzed in 4 $^{\circ}\text{C}$ deionized water. The deionized water was replaced twice a day for 5 days. Finally, the dialysate in the tube was freeze-dried to obtain the DNCPs and stored at $-20\text{ }^{\circ}\text{C}$.

2.2 Identification of DNCPs

DNCPs were detected by Coomassie bright blue staining. DNCPs and loading buffer were mixed and boiled to complete protein denaturation. Sodium dodecyl sulfate–polyacrylamide gel electrophoresis (SDS-PAGE) was performed. Then, the gel was put in Coomassie bright blue staining solution for 30 min. Then, the gel was placed into

the decolorization solution. The gel was photographed and recorded through a gel imaging system (AL600RGB, GE Healthcare, Waukesha, WI, USA).

Then, DNCPs were identified by western blot analysis. DNCPs and loading buffer were mixed and boiled for 5 min. The proteins (40 µg per lane) were separated using a 10% SDS–PAGE gel for electrophoresis. Then, the proteins were transferred to PVDF membranes. The membranes were blocked with 5% bovine serum albumin (BSA) at room temperature for 2 h. DNCPs were specifically bound by primary antibodies (DSPP, 1:1000; DMP1, 1:500; OPN, 1:1000; BMP2, 1:1000, Novus Biologicals, Centennial, CO, USA) overnight at 4 °C. Finally, the membranes were rinsed with tris-buffered saline plus Polysorbate 20 (TBST, TBS + Tween 20) and incubated with horseradish peroxidase (HRP)-labeled goat antirabbit IgG (1:5000, Beyotime, China) at room temperature for 40 min. The images were acquired by an automatic chemiluminescence imaging system (Tanon 5200, Tanon Science & Technology, Shanghai, China).

2.3 Detection of DNCPs affecting cell proliferation

A mouse osteoblast-like cell line (MC3T3-E1) was purchased from the Cell Bank of the Chinese Academy of Sciences (Shanghai, China). 4×10^3 cells were transferred to a 96-well plate. After cells were treated with 0, 1, 2.5, 5, 10, 20, 40, and 80 µg/mL DNCPs for 3 days, the effects of different concentrations of DNCPs on cell proliferation were detected by the cell counting kit-8 (CCK-8). The absorbance was measured with a microplate reader (Enspire, PerkinElmer, Waltham, MA, USA) at a wavelength of 450 nm.

2.4 Detection of DNCPs affecting osteogenic differentiation

Alkaline phosphatase (ALP) activity assay was used to test the effect of DNCPs on osteogenic differentiation. Cells were treated with 0, 1, 2.5, 5, 10, 20, 40, and 80 µg/mL DNCPs for 3 days, using the osteogenic induction medium served as the culture media. After the treatments, cells were lysed using the cell lysis buffer for Western and IP without inhibitors (Beyotime, Shanghai, China), and the cell supernatant was collected in a 96-well plate. ALP activity was evaluated using an Alkaline Phosphatase Assay Kit (Beyotime) and determined at the wavelength of 405 nm. ALP activity was normalized to the total protein content.

2.5 Preparation of odontogenic BCP

The periodontal membrane, pulp, calculus and caries tissue of waste extracted teeth were removed and treated with serial ethanol dehydration, drying at 60 °C. For the first

calcination, the calcination temperature was set at 800 °C as follows: the temperature was gradually increased to 400 °C within 2 h and to 800 °C within 3 h; the temperature was kept at 800 °C for 1 h; then, the temperature was slowly decreased, and the power was turned off at 200 °C. The calcined teeth were put in 0.1 mol/L diammonium hydrogen phosphate solution for 24 h, and then the materials were dried. Second calcination: gradually heating to 400 °C in 2 h; slowly heating at 400–600 °C for 200 min; temperature rise to 800 °C for 1 h; heat preservation at 800 °C for 1 h; 2 h continued heating to 1150 °C; heat preservation at 1150 °C for 2 h; and then the cooling procedure was entered.

After the processing method [36, 37], dental BCP was obtained. Then, Bio-Oss® (Geistlich Bio-Oss, Wolhusen, Switzerland) and β-TCP (Synthetic Bone tissue, Cortex Dental Implants Industries Ltd., Shlomi industrial Zone, Shlomi, Israel) were used as a contrast to compare their phase composition, particle morphology and pore size. The surface morphology of the materials was characterized using a scanning electron microscope (SEM) (GeminiSEM 300, ZEISS, Jena, Germany) at an extra high tension (EHT) of 3 kV after sputter coating with gold (108Auto, Cressington Scientific Instruments UK, Watford, UK).

2.6 X-ray diffraction (XRD) analysis for phase composition

XRD patterns of the three bone graft materials were analyzed using an X-ray diffractometer (Bruker D8 Advance, Bruker, Bremen, Germany) with CuK α radiation at 30 kV and 30 mA. Data were collected in the 2 θ range of 10–80° with scan speeds of 10–20°/min. Quantitative analysis of the materials was carried out using the whole pattern fitting and Rietveld refinement method.

2.7 Brunauer–Emmett–Teller (BET) experiment for pore size

The BET experiment was conducted using nitrogen adsorption on a device (ASAP 2020, GOW-MAC, Bethlehem, PA, USA). The sample was weighed (approximately 0.0534 g) and dried at 120 °C for 5 h. The specific surface area was determined using the BET method. Barrett–Joyner–Halenda (BJH) desorption methods were used to characterize the pore size. The BJH adsorption dV/dlog(w) pore volume curve was analyzed to evaluate the mode pore width.

2.8 Determination of cell adhesion rate and proliferative activity on materials

In this study, the experimental group was a BCP scaffold, and the control materials were DBBM and β-TCP.

Meanwhile, the experimental group and the control group were divided into two subgroups with or without DNCPs, and intragroup comparisons and intergroup comparisons were carried out. Subsequent *in vitro* experiments were conducted according to this grouping, and the concentration of DNCPs was set at 10 $\mu\text{g}/\text{mL}$. A solution of DNCPs in cells culture medium were dropped onto the materials. Prior to cell seeding, the material was prehumidified to allow the protein solution to infiltrate and adsorb to the material as much as possible.

1×10^6 cells were transferred to a centrifuge tube. MC3T3 cells were seeded into the materials, and after 4 h and 24 h of cell culture, the cell-seeded scaffolds were rinsed with phosphate buffer solution (PBS). The cells on the materials were digested with trypsin (Beyotime), and the materials were rinsed several times with the same amount of PBS. Then, the PBS was collected, and the volumes were fixed. Finally, the cell counting apparatus was used for counting, and the cell adhesion rate was calculated.

The cell proliferative activity was quantified using the CCK-8 assay. 2×10^4 cells were transferred to a 24-well plate. After 1, 3, 5 and 7 days of cell culture, CCK solution (Beyotime) was added to each well containing scaffolds and incubated for 2 h at 37 °C. Next, the solution was transferred to a 96-well plate, and the optical density (OD) values were read on a microplate reader (Enspire, PerkinElmer) at 450 nm wavelength.

2.9 Observation of cell morphology on scaffold surface

Scanning electron microscopy (GeminiSEM 300, ZEISS) was used to observe the cell morphology on the scaffold. 1×10^6 cells were transferred to a centrifuge tube. After the cells were seeded on the scaffolds for 1 day and 3 days, the cell-seeded scaffolds were rinsed with PBS, fixed with 4% paraformaldehyde at room temperature for 30 min, dehydrated with graded ethanol (30–100%), and then treated with tert-butanol twice before critical point drying. Prior to SEM analysis, a conductive film was coated on the surface of the sample with an ion sputter coater (108Auto, Cressington). The cell-seeded scaffolds were analyzed at appropriate magnification to assess the morphology of adherent cells.

2.10 ALP activity assay of cells seeded on the materials

2×10^4 cells were slowly and evenly seeded on the material in a 24-well plate, allowing the cell suspension to fully penetrate the material pores. The scaffolds seeded with cells were cultured for 4 h to facilitate cell adhesion,

and then osteogenic induction solution was added to continue culture. On days 3, 6, and 12, the samples were treated with lysates and the resulting cell suspension was collected into 96-well plates. ALP activity was evaluated using an Alkaline Phosphatase Assay Kit (Beyotime) and determined at the wavelength of 405 nm.

2.11 Maxillary sinus lifting procedures

Nine New Zealand male white rabbits (2.5–3 kg) were used in the study. The protocol for this research was approved by the Animal Research Committee of Anhui Medical University (LLSC 20,210,681). Eighteen maxillary sinus lifting surgeries were performed. Each rabbit was randomly assigned to the DBBM group, β -TCP group and odontogenic BCP group, and the bilateral maxillary sinuses of each rabbit were randomly assigned to the DNCP group and control group. Each sinus was grafted with 0.1 cc of bone substitutes. The particle size of the three materials was typically 0.25–1 mm. Six hours prior to surgery, 1 mg/mL DNCP solution was added to the material to fully soak it. The rabbits were anesthetized with 3% pentobarbital sodium (1 mL/kg) intravenously. In addition, 0.5–1 mL mepivacaine was injected subcutaneously into the field of operation for infiltration anesthesia. Then, a vertical incision approximately 2.5–3 cm along the midline of the nasal dorsum was made, and the skin and subcutaneous tissue were incised to expose the nasal bone on both sides. With a round drill, two 5 mm round bone windows located approximately 0.5 cm laterally to the midline of the nasal dorsum, 2 cm in front of the sutura nasofrontalis, were prepared during continuous cooling with saline solution. The sinus mucosa was exposed by careful operation. Perforation of the Schneiderian membrane was not observed during surgery. The thin bone fragments were temporarily kept in saline solution. Then, the two bone windows were filled with bone substitutes. Bone substitutes loaded with DNCPs were grafted into one sinus (the DNCP subgroup), and saline-soaked bone substitutes were placed into the other (the control subgroup) in each rabbit. Then, the thin bone fragments were replaced with the bone window. Finally, the subcutaneous tissue and skin were sutured separately. Antibiotics were administered for 3 days after surgery (Supplementary Fig. S1A–F).

At the end of the 4-month implantation time, the rabbits were sacrificed by an overdose of pentobarbital sodium given intravenously. The maxilla was immediately removed and fixed in 10% formalin solution. The maxillary specimen is shown in Supplementary Fig. S1G, and the histological section clearly demonstrated the correct location and effectiveness of maxillary sinus elevation. (Supplementary Fig. S1H).

2.12 Micro-CT scanning

Microcomputed tomography (Micro-CT) (SkyScan 1176, Bruker) was used to assess new bone formation in rabbit maxillary sinus lifting. The parameters of new bone quality and quantity were acquired through a micro-CT analysis system (CTvox, Bruker), such as tissue volume (TV), the ratio of bone volume to total volume (BV/TV), trabecular thickness (Tb. Th), trabecular number (Tb. N), trabecular separation (Tb. Sp), structure model index (SMI), and bone mineral density (BMD).

2.13 Histological analyses

The specimens were dehydrated in a gradient of 70–100% ethanol and embedded (without decalcification) in methyl methacrylate (MMA). After embedding, thin sections were prepared and stained with Goldner's trichrome stain (Servicebio Technology Co., Ltd., Wuhan, China) to obtain a histological view of the maxillary sinus area. Histologic observation was performed using a panoramic slice scanner (PANNORAMIC DESK/MIDI/250/1000, 3DHISTECH, Budapest, Hungary) and scan browsing software (CaseViewer2.4, 3DHISTECH). All sections were quantitatively evaluated using Image-Pro Plus software (Media Cybernetics, Rockville, MD, USA) and ImageJ software (National Institutes of Health, Bethesda, MD, USA). The following parameters were measured within the region of interest (ROI) for histomorphometric analysis: 1. Highly mineralized bone (dark green area as a proportion of the total area); 2. Dark green average IOD (IOD: integral optical density. Dark green average IOD: dark green area IOD/dark green area, that can indirectly reflect bone density and degree of mineralization); 3. Low mineralized bone (light green area as a proportion of the total area); 4. Light green average IOD (light green average IOD: light green area IOD/light green area); 5. New bone area (green area as a proportion of the total area).

2.14 Statistical analysis

Statistical analyses were performed with SPSS software (IBM SPSS Statistics 20.0, Chicago, IL, USA) and GraphPad software (GraphPad Prism 8.2.1, San Diego, CA, USA). One part used one-way analysis of variance (ANOVA), and the other used two-way ANOVA with Tukey–Kramer multiple comparisons test and Sidak's multiple comparisons test. All the data are expressed as the mean \pm standard deviation. Differences at $*p < 0.05$ were considered significant.

3 Results

3.1 Identification analysis of DNCPs

The extracted DNCPs showed a thin film after lyophilization (Fig. 1A). Coomassie blue staining results showed that the molecular weight distribution of the protein samples had the following characteristics: 1. An obvious blot was seen near 70 kDa; 2. Clear blots could be seen at approximately 55 kDa, 130 kDa and above 180 kDa, which might be DSPP, DMP1, BMP2 and other proteins [30, 31, 35]. Because this test can only measure protein molecular weight, we can only make some conjectures based on DNCPs itself, and the results can only be used for auxiliary verification (Supplementary Fig. S2).

Western blot results showed that the DNCP extract contained and expressed DSPP (NBP2-92,546, Theoretical molecular weight: 131 kDa), DMP1 (NBP1-45,525, Theoretical molecular weight: 130 kDa), OPN (NB110-89062SS, Theoretical molecular weight: 75 kDa) and BMP2 (NBP1-19751SS, Theoretical molecular weight: 44 kDa) (Fig. 1B). The molecular weight of proteins may vary from the predicted molecular weight due to the extraction process, protein phosphorylation and other protein modification factors [38, 39].

3.2 DNCPs optimum concentration

The CCK-8 assay showed that compared with the 0, 1, 2.5, 5, and 10 $\mu\text{g}/\text{mL}$ DNCP groups, the OD value of the 80 $\mu\text{g}/\text{mL}$ group was statistically different ($*p < 0.05$). The cell proliferation curve also shows that there was no significant difference between the groups below 10 $\mu\text{g}/\text{mL}$, but 10 $\mu\text{g}/\text{mL}$ DNCPs significantly promoted the ALP activity ($*p < 0.05$). However in 20 $\mu\text{g}/\text{mL}$ group, ALP activity decreased notably ($*p < 0.01$). In 40 and 80 $\mu\text{g}/\text{mL}$ group, ALP activity was significantly lower than the control group, the difference was statistically significant ($*p < 0.0001$). When the concentration of DNCPs ranged from 10 to 80 $\mu\text{g}/\text{mL}$, both cell proliferation and ALP activity showed a downward trend (Fig. 1C, D).

In addition, during the determination of protein concentration, we also found that the extracted DNCPs were not pure and may contain substances that affect cell viability, such as residual protease inhibitors. Therefore, improvement of the extraction method is needed. In subsequent in vitro experiments, 10 $\mu\text{g}/\text{mL}$ was used as the optimal concentration.

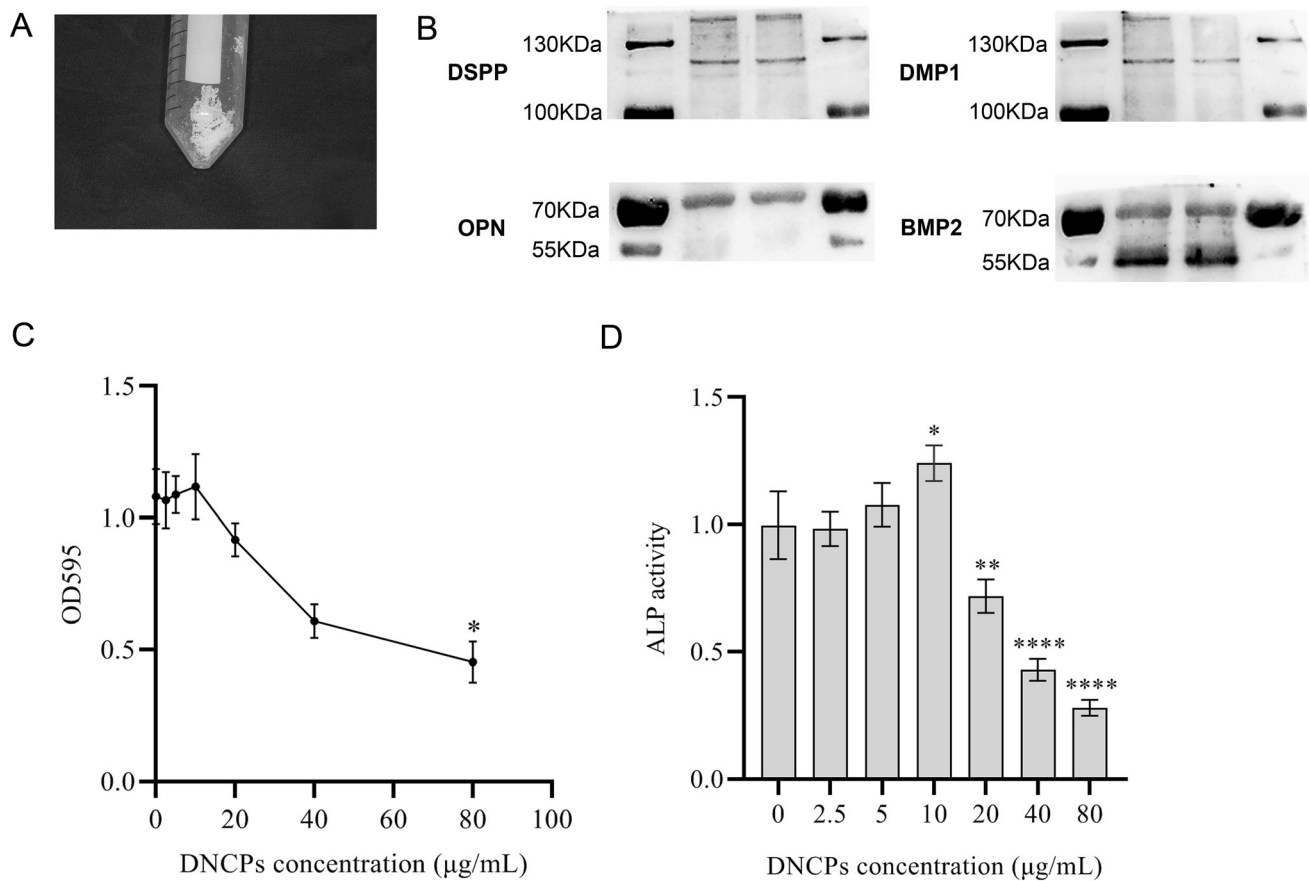


Fig. 1 Experiment detection about DNCPs. **A** The extracted DNCPs showed a thin film after lyophilization. **B** Western blot results. **C** DNCPs optimum concentration was tested by CCK8 method; the abscissa corresponding to the points are 0, 1, 2.5, 5, 10, 20, 40, 80; *

statistic difference compared with 0, 1, 2.5, 5, 10 µg/mL DNCPs, $p < 0.05$. **D** DNCPs optimum concentration was tested by ALP activity assay; * statistic difference compared with 0 µg/mL DNCPs; (* $p < 0.05$, ** $p < 0.01$, *** $p < 0.001$ and **** $p < 0.0001$)

3.3 XRD phase identification

As shown in Fig. 2A, the tooth powder sintered for the first time was gray and white. However, the material treated with ammonium dihydrogen phosphate was sintered for the second time, and then a white powder was obtained. Figure 2B–E shows the XRD diffractograms of dental powder sintered for the first time (Fig. 2B) and the second time (Fig. 2C), DBBM (Fig. 2D) and β -TCP (Fig. 2E). The detected phases corresponded to BCP (a 87/13 mass fraction of HA and β -TCP), BCP (a 71/29 mass fraction of HA and β -TCP), HA and β -TCP respectively. HA (PDF#84–1998) and β -TCP (PDF#09–0169) are the standard powder diffraction file (PDF) cards.

After the first sintering, the tooth powder had the characteristics of HA diffraction peaks and some specific diffractive peaks of β -TCP. And at the second sintering, part of HA was transformed into β -TCP. Because the sintering temperature was below 1200 °C, no α -TCP phase was produced, which was also confirmed by the diffraction pattern. Although the intensity of the β -TCP diffraction

peak of odontogenic BCP was weaker than the intensity of the β -TCP diffraction peak of the standard pattern (PDF#09–0169), the intensity ratio of the main diffraction peaks were consistent with the standard characteristics. But the diffraction peaks of the β -TCP deviated to little angle, to be exact, this substance was $\text{Ca}_{2.71}\text{Mg}_{0.29}(\text{PO}_4)_2$ (PDF#70–0682), calcium ion was replaced by magnesium ion in teeth, a small quantity of magnesium ions entered into the lattice. Because of the focus of this study on the effect of odontogenic and biphasic calcium phosphate material as scaffold, besides, teeth naturally contain magnesium and this ion replacement is inevitable, we still refer to it as β -TCP rather than $\text{Ca}_{2.71}\text{Mg}_{0.29}(\text{PO}_4)_2$.

3.4 BET test results

The isotherm linear plots of these three materials had similar characteristics. They were all type IV isotherms and mesoporous materials. The adsorption curve was inconsistent with the desorption curve, and hysteresis rings were observed. Moreover, the three materials were all H3 type

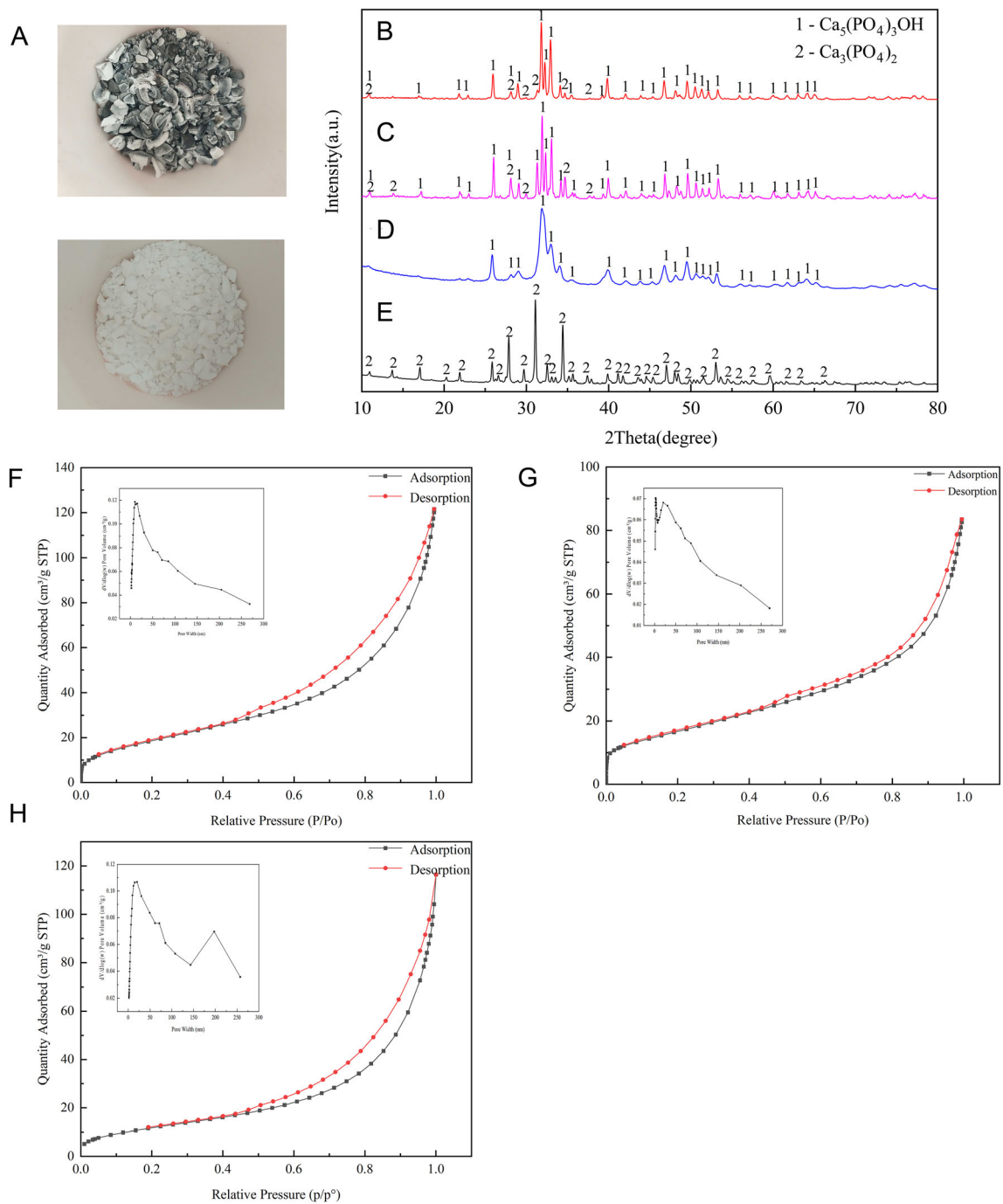


Fig. 2 Materials testing. **A** Dental powder materials images after the first and second sintering. **B** XRD pattern of dental powder after the first sintering. **C** XRD pattern of odontogenic BCP. **D** XRD pattern of DBBM. **E** XRD pattern of β -TCP. **F** Isotherm linear plot and BJH

adsorption $dV/d\log(w)$ pore volume plot of DBBM. **G** Isotherm linear plot and BJH adsorption $dV/d\log(w)$ pore volume plot of β -TCP. **H** Isotherm linear plot and BJH adsorption $dV/d\log(w)$ pore volume plot of BCP

without an obvious saturated adsorption platform, indicating that these materials were flake or granular, with fissure pore characteristics and irregular pore structure. Figure 2F–H was used to obtain the mode pore width.

Table 1 summarizes the BET surface area, pore volume, average pore size, mode pore width, median micropore

width of DBBM, β -TCP and odontogenic BCP. (Note: All three materials were tested after hand grinding and refinement, and their data, such as specific surface area, may change. The results of DBBM and β -TCP materials were used only for comparison in this study and could not be evaluated clinically).

Table 1 Brunauer Emmett Teller (BET) test results of the three materials

Material	BET surface area (m ² /g)	Pore volume (cm ³ /g)	Average pore size (nm)	Mode pore width (nm)	Median micropore width (nm)
BCP	50.7011 ± 0.5316	0.148567	10.5516	20.3386, 200	1.0606
DBBM	69.7139 ± 0.8513	0.176995	8.4611	10.0113	1.0381
β-TCP	60.6485 ± 0.4891	0.122344	7.4471	2.9414, 20.6371	1.0387

BET, Brunauer–Emmett–Teller; BCP, biphasic calcium phosphate; DBBM, deproteinized bovine bone mineral; β-TCP, β-tricalcium phosphate

Although the specific surface area of BCP was the smallest among the three, BCP had the largest average pore size of 10.5516 nm. The mode pore width represents the most likely pore size, which is a concept of probability. The mode pore widths of BCP were 20.3386 and 200 nm, and the 200 nm macropores may be densely distributed dentin tubule-like pores on the surface of BCP. In addition, all three materials had micropores of approximately 1 nm.

3.5 Material morphological observation

Figure 3 shows representative scanning electron microscopy (SEM) images of the material surfaces. The odontogenic BCP presented two main surface characteristics: one was a smooth surface with dentin tubule-like traffic pores, and the other was a granular structure of approximately 1 μm. SEM images of DBBM and β-TCP materials

showed that the surface of the material had large ovoid megapores of approximately 50–200 μm (Supplementary Fig. S3). Higher SEM magnification revealed clear differences in the nanostructure features. The surface of DBBM presented as thick uniform, while β-TCP is characterized by irregular granules. However, schistic and scaly irregular crystals, as well as irregular pores with hundreds of nanometer diameters, were observed in BCP.

3.6 Biocompatibility analysis of materials and DNCPs

The results of the cell adhesion experiment showed that DNCPs had no significant effect on cell adhesion. Compared with the DBBM group, the cell adhesion rate of the β-TCP group was significantly higher at both 4 h and 24 h. While the 24 h adhesion rate of the BCP Group was lower

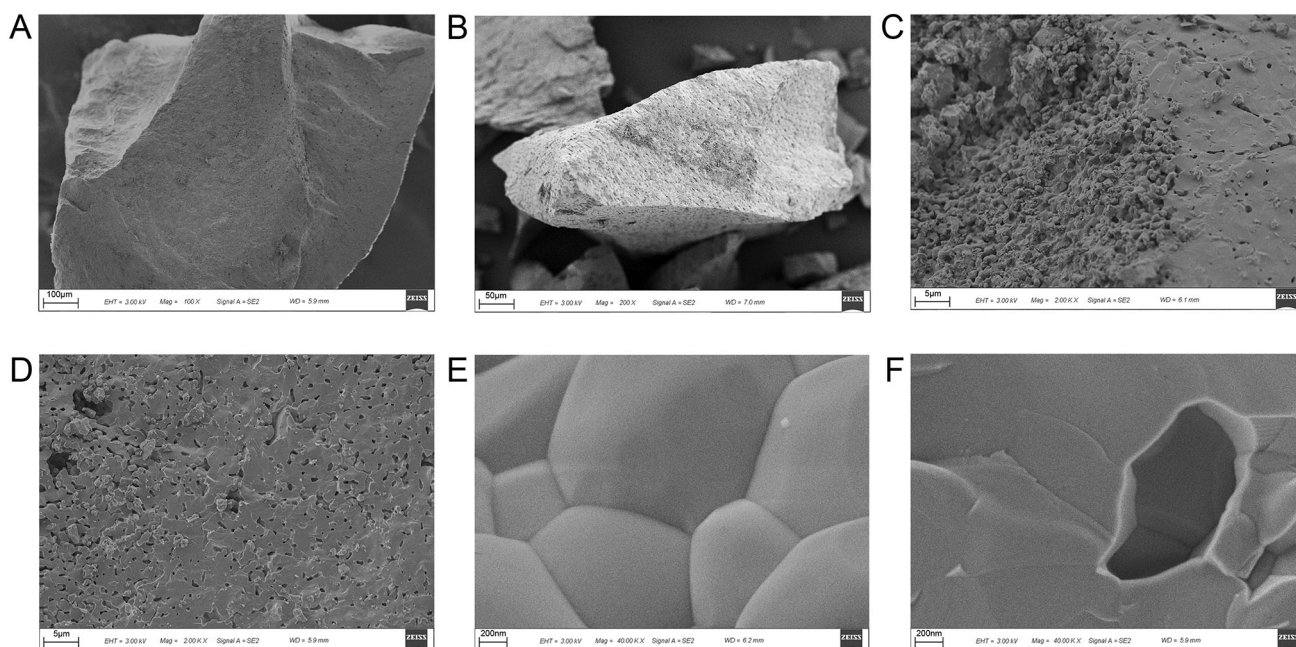


Fig. 3 SEM images of BCP. **A** Material surface under low magnification (Mag = 100X). **B** Porous surface under low magnification (Mag = 200X). **C** Two kinds of microscopic morphology

(Mag = 2kX). **D** Representative microscopic morphology (Mag = 2 kX). **E** Micro-nanostructured features (Mag = 40kX). **F** Representative nanoscale pore structures (Mag = 40kX)

than the 24 h adhesion rate of the DBBM group and the β -TCP group, the differences were statistically significant (Fig. 4A).

From day 1 to day 7, the proliferation of cells in each group increased continuously. The data showed that the number of cells in all groups was similar on days 1 and 3, and the difference was not statistically significant. However, from day 5, the number of adherent cells on the β -TCP scaffold was statistically the highest, significantly different compared with both the DBBM and BCP groups. In addition, DNCP stimulation had no noteworthy effect on cell proliferation, and 10 μ g/mL DNCPs did not exhibit cytotoxicity (Fig. 4B).

3.7 Cell spreading and morphology observation

The SEM tests showed images of 3T3 cells cultured on BCP (Fig. 5), DBBM (Supplementary Fig. S4A–D) and β -TCP materials (Supplementary Fig. S4E–H) in the presence or absence of DNCPs. Cell spreading and morphology were analyzed by high magnification images. In order to observe the cell adhesion and spreading on material particles, laser scanning confocal microscope (LSCM) observation were performed simultaneously, experimental procedure and results are shown in Supplementary Fig. S5 and S6.

Observing the materials seeded cells by SEM for 1 d, we found that the cells on the DBBM and β -TCP scaffolds

were fusiform or oval and extended elongated filopodia to adhere to the materials, and some cells began to spread out to enhance the adhesion to the substrate materials. The images on day 3 revealed that the cell spread area increased, the proliferation of cells increased, and there was a tendency of concentrated growth in some locations. On the BCP scaffolds, the cells were widely spread, and confluent layers were formed. Especially on culture day 3, numerous filopodia could be seen sticking out around the cells, indicating that the BCP material had good contact and adhesion with cells.

3.8 Effect of materials on ALP activity

The ALP activity of cells in each material group increased with time (Fig. 4). On day 3, 6, 12, the ALP activity of β -TCP group was significantly higher, compared to the DBBM group ($*p < 0.05$). On day 3, there was no significant difference in ALP activity between DBBM group and BCP group ($*p > 0.05$). Cultured to 6 days, 12 days, ALP activity of BCP group was higher than DBBM group, the difference was statistically significant ($*p < 0.05$).

3.9 Micro-CT analysis

The micro-CT scanning images (three-dimensional reconstruction image, axial image, sagittal view) presented dome-shaped bone lifting consisting of new bone and

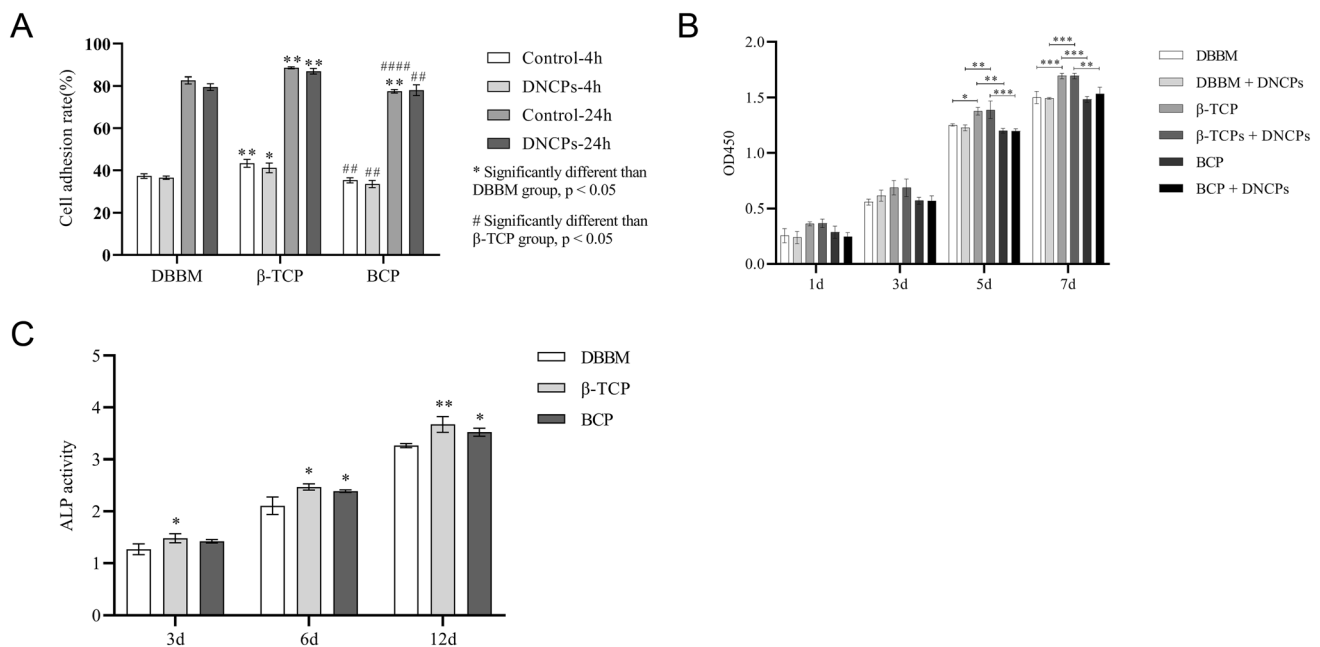


Fig. 4 Cell adhesion rate, proliferative activity and ALP activity. **A** Determination of cell adhesion rate (* Significantly different than DBBM group, $p < 0.05$; # Significantly different than β -TCP group, $p < 0.05$). **B** Cell proliferative activity detection. (* Significantly

different than β -TCP group, $p < 0.05$), ($*p < 0.05$, $**p < 0.01$, $***p < 0.001$ and $****p < 0.0001$). **C** ALP activity assay. (* Significantly different than DBBM group, $p < 0.05$), ($*p < 0.05$, $**p < 0.01$)

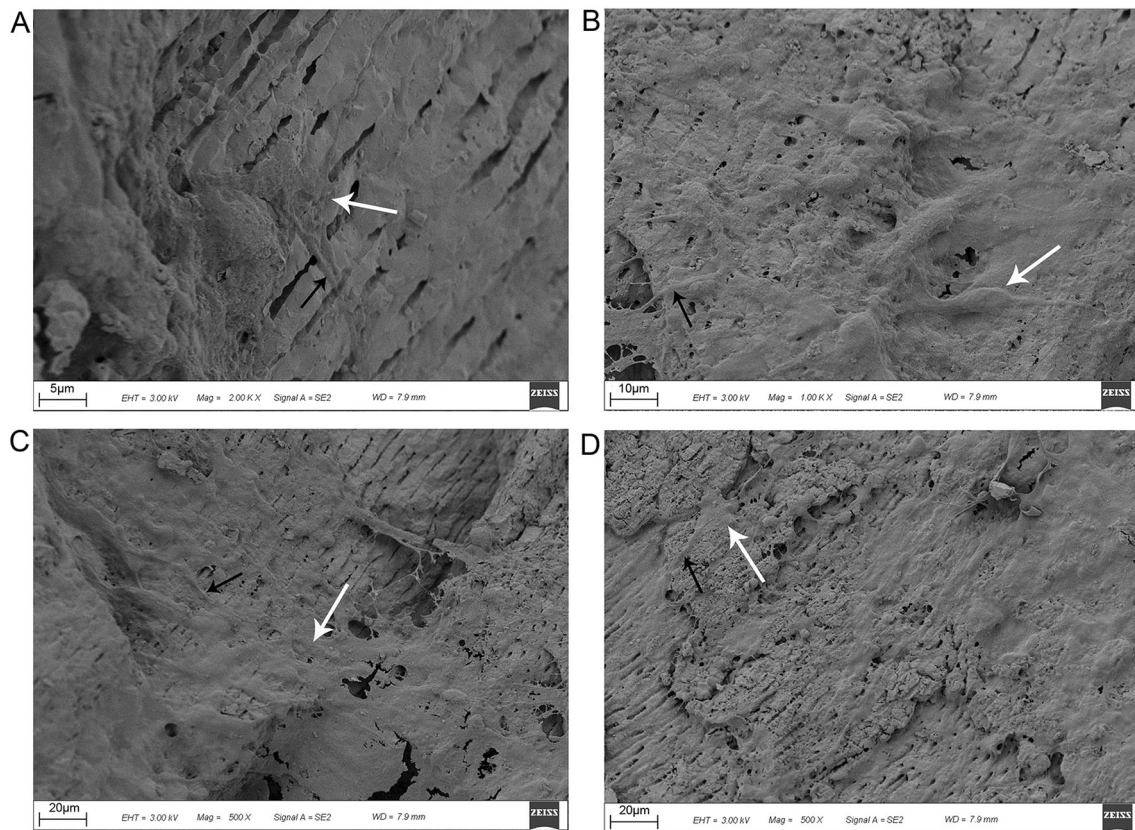


Fig. 5 Cell morphology SEM observation. **A** BCP, day 1. **B** BCP + DNCPs, day 1. **C** BCP, day 3. **D** BCP + DNCPs, day 3. (White arrow: cell. Black arrow: filopodia)

residual material in the rabbit maxillary sinus (Fig. 6). The images revealed that the β -TCP material had largely degraded after 4 months of healing, while the residual material of DBBM and BCP was in close contact with the new bone. The values of parameters are listed in Supplementary Table S1. Statistical results of two-way ANOVA are shown in Supplementary Table S2.

The TV (mm^3) values were 67 ± 6.03 , 42.7 ± 2.92 , 64.3 ± 3.82 , 68.96 ± 2.08 , 47.62 ± 1.74 and 70.34 ± 4.11 in the DBBM-Control, β -TCP-Control, BCP-Control, DBBM-DNCPs, β -TCP-DNCPs and BCP-DNCPs groups, respectively. The results showed that there were significant differences between DBBM and β -TCP, β -TCP and BCP. However, there were no statistically significant differences between the control subgroup and DNCP subgroup in any of the three materials (Fig. 7). The BV/TV (%) values of β -TCP and BCP were 47.18 ± 5.68 and 62.62 ± 7.02 in the DNCP groups, respectively, and they were significantly different. BCP-Control and BCP-DNCPs showed BV/TV values of 42.56 ± 7.80 and 62.62 ± 7.02 , respectively; significant differences were detected (Fig. 7B). The Tb. Th (μm) value in the BCP-DNCP group (303.9 ± 34.95) was notably greater than the Tb/Th (μm) value in the β -TCP-DNCP group (225.3 ± 40.80). There

were no significant differences among the other groups (Fig. 7C). The Tb. Sp of DBBM (470.3 ± 56.91) and BCP (429.4 ± 22.03) were significantly different compared with β -TCP (608.9 ± 55.57) in the control group. For β -TCP and BCP materials, there were also significant differences between the control and DNCP subgroups (Fig. 7E). Two-way ANOVA did not show Tb. N, SMI or BMD differences in the material groups or the control-DNCP subgroup (Fig. 7D, F and G). Interestingly, the SMI for all material and protein groups was close to 0, indicating that most bone trabeculae were lamellar, and negative number represented dense structure.

3.10 Histological results

Histological slices show Goldner's trichrome staining of the maxillary sinus bone lifting area 4 months after the operation (Fig. 8). The images showed that dark green highly mineralized and light green low mineralized new bone was formed in contact with the surface of the bone substitutes and had a bone trabecular structure. Low mineralized bone exhibited woven bone trabeculae, while the presence of lamellar bone was an indication of bone maturity. Osteoblasts were observed on a low mineralized

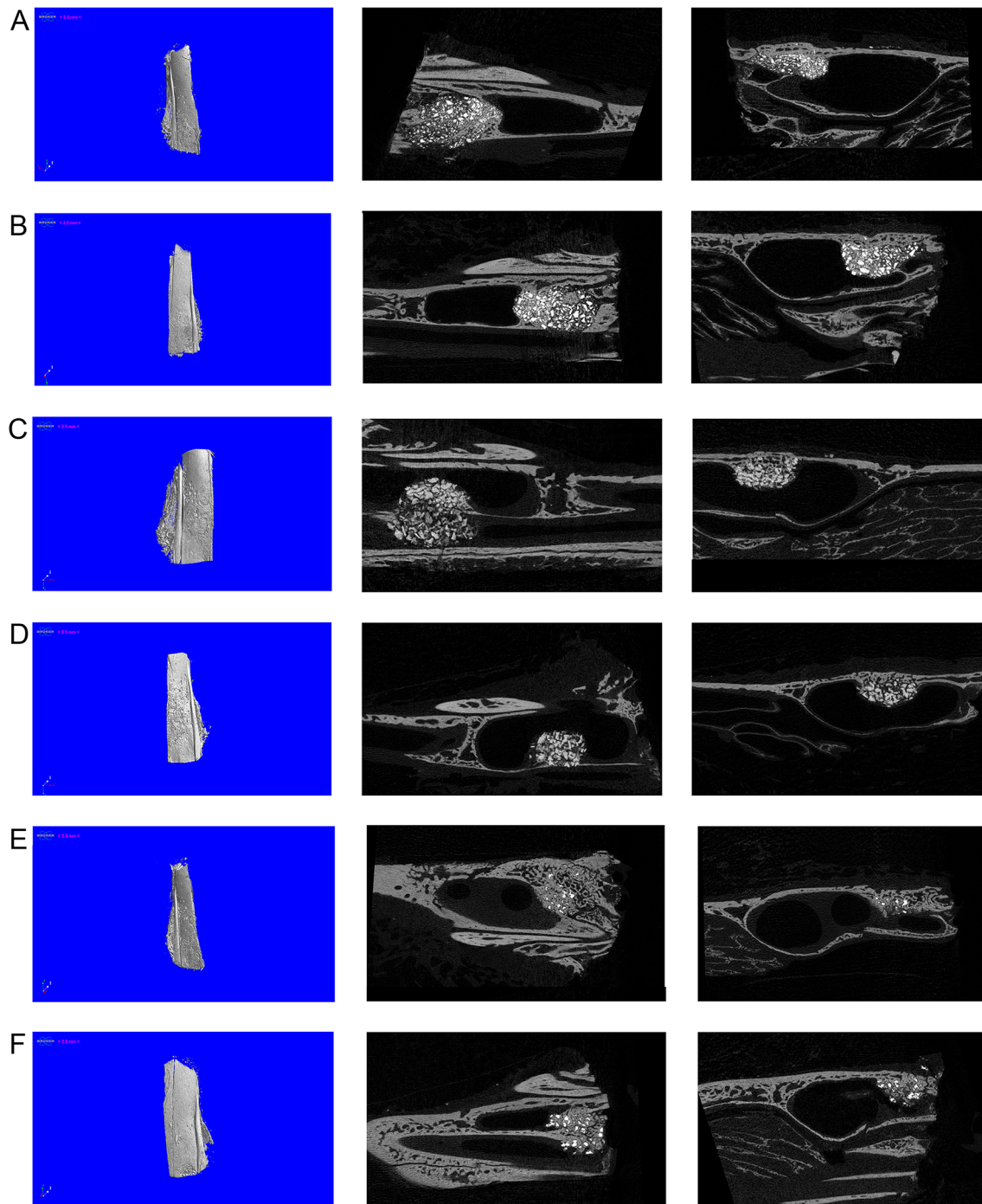


Fig. 6 Micro-CT scanning images (three-dimensional reconstruction image, axial image, sagittal view). **A** BCP-Control group. **B** BCP-DNCPs group. **C** DBBM-Control group. **D** DBBM-DNCPs group. **E** β -TCP-Control group. **F** β -TCP- DNCPs group

new bone surface. Some areas were orange-red, and these were unmineralized osteoids. Residual DBBM and BCP could be distinctly observed, indicating that these materials were not fully degraded at 4 months, while β -TCP was clearly degraded compared with them. After four months of healing, only a few β -TCP granules were scattered in the bone. In both the experimental and control groups, there

was new bone formation in the central area, surrounding area and around the sinus membrane, demonstrating the osteoconduction properties of these materials. The new bone was in close contact with the material surface, some irregular material surfaces may be caused by the degradation of material particles.

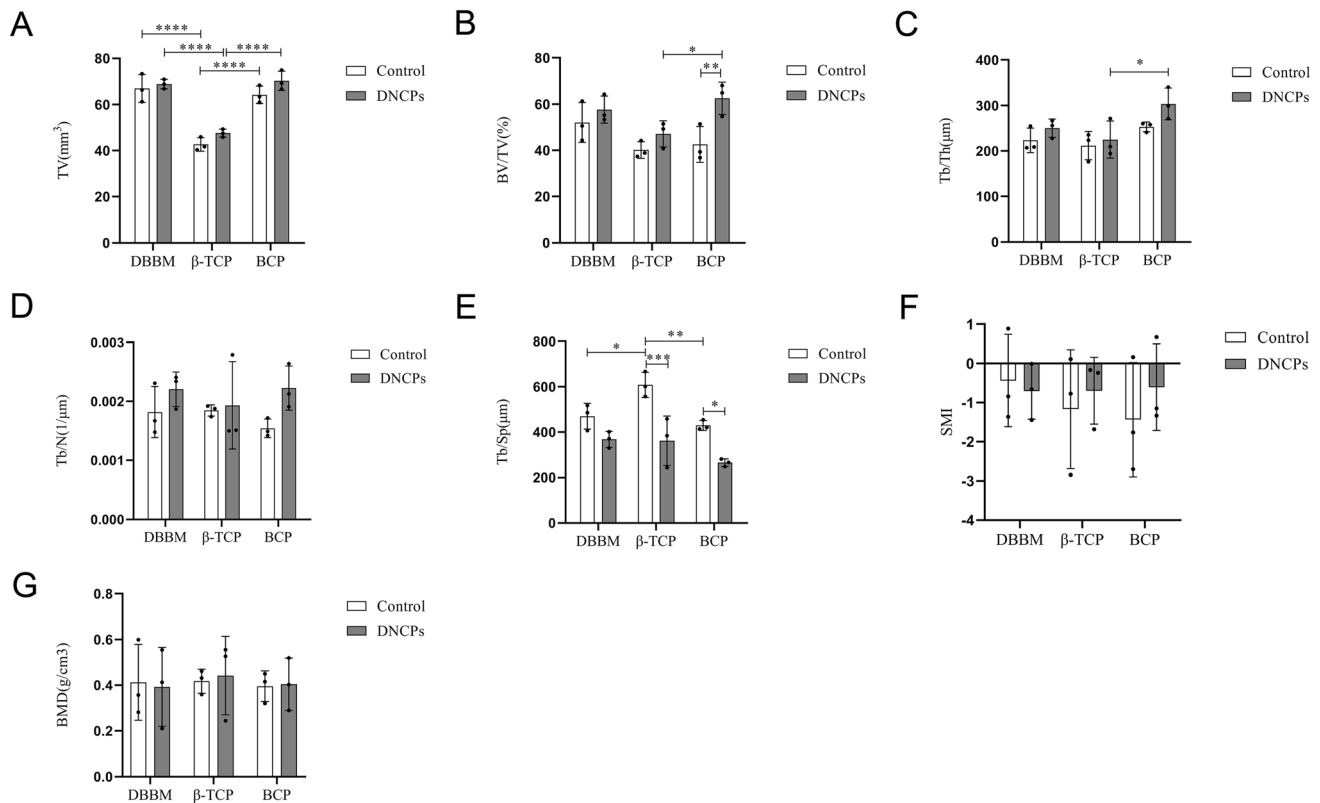


Fig. 7 Micro-CT analysis. **A** Tissue volume (TV). **B** the ratio of bone volume to total volume (BV/TV). **C** trabecular thickness (Tb.Th). **D** trabecular number (Tb.N). **E** trabecular separation (Tb.Sp).

F structure model index (SMI). **G** bone mineral density (BMD). (* $p < 0.05$, ** $p < 0.01$, *** $p < 0.001$ and **** $p < 0.0001$)

Histomorphometric results are shown in Supplementary Table S3 and Supplementary Table S4. The amounts of highly mineralized bone (%) were 28.73 ± 4.549 , 24.10 ± 5.051 , 26.13 ± 8.210 , 27.20 ± 14.94 , 34.63 ± 3.607 and 25.70 ± 12.21 in the DBBM-Control, β -TCP-Control, BCP-Control, DBBM-DNCPs, β -TCP-DNCPs and BCP-DNCPs groups, respectively. There were no significant differences among these groups (Fig. 9A). The values of dark green average IOD were not significantly different among the material groups. Between BCP-Control and BCP-DNCPs, β -TCP-Control and β -TCP-DNCPs, significant differences were detected (Fig. 9B). The amounts of low mineralized bone (%) were 42.33 ± 4.250 , 38.47 ± 11.58 , 48.40 ± 4.828 , 42.27 ± 5.519 , 41.00 ± 4.949 and 51.77 ± 13.45 in the DBBM-Control, β -TCP-Control, BCP-Control, DBBM-DNCPs, β -TCP-DNCPs and BCP-DNCPs groups, respectively (Fig. 9C). No statistical differences were found among the groups. The values of light green average IOD did not differ significantly between the material groups. However, in the DBBM and BCP groups, there were prominent differences between the control and DNCP subgroups (Fig. 9D). The new bone area (%) values were 71.07 ± 1.193 , 62.57 ± 6.730 , 74.53 ± 3.661 ,

69.47 ± 9.445 , 75.63 ± 1.380 and 77.47 ± 3.156 in the DBBM-Control, β -TCP-Control, BCP-Control, DBBM-DNCPs, β -TCP-DNCPs and BCP-DNCPs groups, respectively. The BCP-Control and DBBM-Control groups exhibited a greater new bone area than the β -TCP-Control group at 4 months of healing, and the differences were significant. In addition, the new bone area was significantly smaller in the β -TCP-Control group than in the β -TCP-DNCPs group (Fig. 9E).

4 Discussion

The utilization of scaffold material delivering growth factors to facilitate tissue-engineered osteogenesis takes a large step forward in maxillary sinus lifting [40–43]. It is desirable that scaffolds and growth factors be designed to mimic the structure and properties of the bone matrix. The main work of this study was to prepare calcium phosphate bioceramics adsorbing DNCPs, to evaluate the volume stability after maxillary sinus elevation and to examine whether the material differences and the addition of DNCPs ultimately affected new bone formation after 4 months of healing.

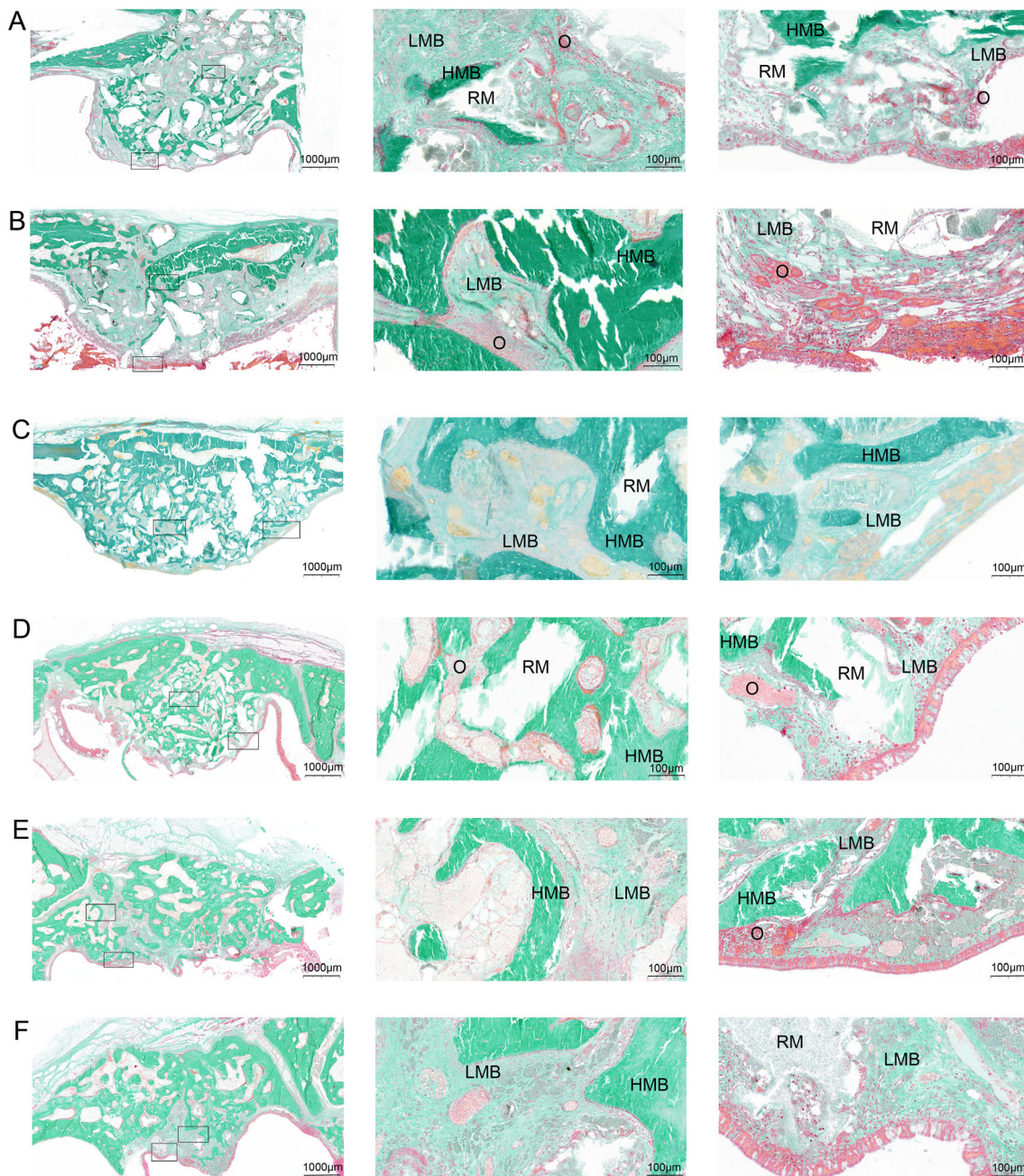


Fig. 8 Histological images. **A** BCP-Control group. **B** BCP-DNCPS group. **C** DBBM-Control group. **D** DBBM-DNCPS group. **E** β -TCP-Control group. **F** β -TCP -DNCPS group. Magnified images were

taken at two locations, one around the defect center and one near the sinus membrane. (Highly mineralized bone: HMB; Low mineralized bone: LMB; Osteoid area: O; Residual material: RM)

We considered, on the one hand, that DNCPS act as biosignal molecules in tissue engineering; on the other hand, DNCPS may participate directly in the formation of bone structure. Previous reports showed that the synergistic effect of growth factors plays a crucial role in bone defect repair [44–46]. Chen et al. evaluated bone regeneration as a highly coordinated process that requires a series of growth factors to be expressed in a spatiotemporally controllable manner [47]. The signal transduction activated

by growth factors may participate in bone reconstruction. The excellent mechanical properties of bone are due to its complicated nanostructure, which contains collagen, minerals and NCPs [23]. NCPs are considered signaling molecules in bone formation and further impact the mineralization of the bone matrix [24, 48]. The crucial factor affecting bone matrix quality is exactly bone matrix mineralization. Some studies suggest that NCPs play a similar “glue” role at the collagen-mineral interface and

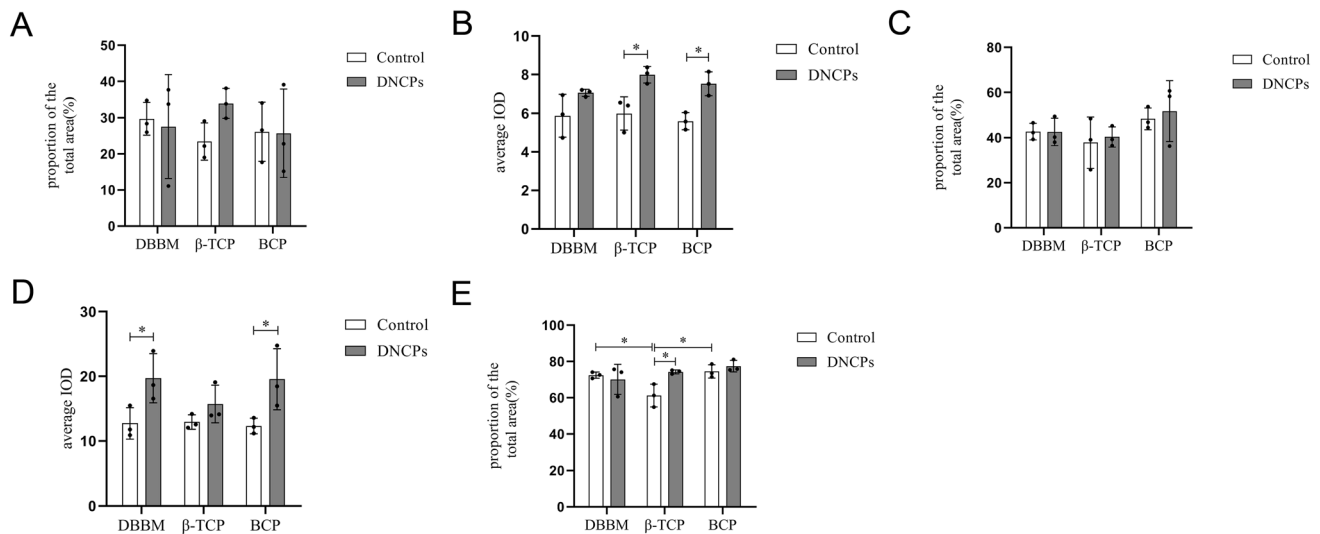


Fig. 9 Histological analysis. **A** Highly mineralized bone area (%). **B** Dark green (represent highly mineralized bone) average IOD. **C** Low mineralized bone area (%). **D** Light green (represent low

mineralized bone) average IOD. **E** New bone area (%) (highly mineralized bone area + low mineralized bone area). (* $p < 0.05$)

strengthen toughness, moreover NCPs can guide calcium phosphate deposition and promote the formation of hydroxyapatite crystals [24, 26, 49–51].

Mineral deposition *in vivo* is not only affected by the inorganic phase but also controlled by protein adsorption [52]. If more proteins that promote osteogenic differentiation are adsorbed, better bone repair may be achieved. Wang et al. found that BCP scaffolds exhibited more BMP2 protein adsorption than HA [53]. The odontogenic BCP material showed good bone formation, which may be related to the phase composition, material surface properties, and pore size. The chemical composition of the material represents a scaffold rich in calcium and phosphorus ions. Appropriate pore size and porosity contribute to the nutrition, colonization, and proliferation of cells associated with osteogenesis. The surface characteristics of materials may affect the specific surface area of materials, thereby affecting the adhesion of cells, proteins, growth factors, etc. BCP ceramics not only have good biocompatibility and bone conductivity but also have slow absorption of HA to maintain space for bone reconstruction, furthermore, the progressive degradation of β -TCP in BCP particles and subsequent release of calcium/phosphorus ions lead to effective mineral deposition in the space after material absorption [7, 54]. These mineral deposits form carbonate HA (CHA), which promotes the adhesion of osteogenic cells and proteins to the material and accelerates the synthesis of bone matrix and the formation of osteoids [55].

In this study, combined with micro-CT scanning images and tissue section observations, β -TCP material did not maintain the height of maxillary sinus bone lifting, and

most of the material had degraded after the healing period of 4 months. The volume of sinus lift (100 mm^3) dropped below 50 mm^3 (TV, β -TCP-Control: 42.7 ± 2.92 ; β -TCP-DNCPs: 47.62 ± 1.74), less than half. However, in the maxillary sinus elevation model with DBBM and BCP materials as scaffolds, dome-shaped protrusions were obvious. In terms of new bone formation, the BV/TV of the BCP-DNCPs group was higher than the BV/TV of the BCP-Control group and β -TCP-DNCPs group; however, there was no significant difference between the BCP group and DBBM group, this result indicated that these two materials can achieve good bone formation, but the effect of β -TCP materials was slightly less. The microstructure of bone trabeculae could reflect the bone quality, and the porous network structure connected by bone trabeculae was arranged regularly according to the stress curve, which could increase the strength. The Tb. Sp values of the DBBM, BCP groups and DNCP subgroups were significantly smaller, suggesting higher bone quality. Histological quantitative analysis showed that there was no significant difference in high or low mineralized bone area among groups, and individual differences were also large, but the percentage of total new bone area in the β -TCP-Control group was significantly lower than the percentage of new bone area in the DBBM-Control group and BCP-Control group. Although the average IOD values of the green area, which indirectly indicated the degree of mineralization, showed no significant difference among the different material groups, significant differences in IOD values were observed between the DNCP and control subgroups in all three material groups, indicating that the presence of DNCPs may contribute to the mineralization of the bone

matrix. The two-way ANOVA results of both micro-CT and histological analysis showed that different material groups had a significant impact on the experimental results, as did the DNCP group, but the interaction between the two factors was found only in the new bone area index of histological analysis. In conclusion, both BCP material and DNCPs played a promoting role in the outcome of bone formation after maxillary sinus lifting in this study.

The odontogenic BCP scaffolds composed of 71% HA and 29% β -TCP were prepared by a sintering technique. The tooth powder sintered for the first time was identified by XRD as HA with a small number of β -TCP (13%). The material treated with ammonium dihydrogen phosphate was sintered for the second time, and then the odontogenic BCP (71% HA and 29% β -TCP) was obtained. When calcined at high temperature, HPO_4^{2-} was converted to $\text{P}_2\text{O}_7^{4-}$, which reacted directly with OH^- in HA to form PO_4^{3-} . The surface of the DBBM and β -TCP material had large ovoid megapores of approximately 50–200 μm . Pore sizes between 150 and 500 μm are most suitable for bone ingrowth [56]. However, the odontogenic BCP was sintered from massive tooth fragments, which did not form hundreds of micron pores. In addition, in BET detection, the BET surface area was lower, and the particle size and shape of the odontogenic BCP materials may reduce the specific surface area. However, its pore volume, average pore size and median micropore width were not very different from those of DBBM and β -TCP. These micropores formed by sintering, can transport nutrients, oxygen and waste for cell growth within the scaffolds, and promote the protein adhesion [57, 58]. *In vitro* experiments, ALP activity of cells seeded on the material was significantly higher in BCP group and β -TCP group, compared to the DBBM group. And the cell adhesion and proliferation of BCP and DBBM were significantly lower the adhesion and proliferation of β -TCP, but SEM and LSCM images (Supplementary Figure S5–S6) showed that the morphology and spread of the cells in the three groups of materials were all outstanding, and an abundance of filamentous pseudopods was found, indicating high biological activity. Combined with the results of *in vivo* experiments, the shortcomings of some parameters of odontogenic BCP did not affect its excellent bone regeneration effect. The cell adhesion rate and proliferation activity of odontogenic BCP material were lower than that of β -TCP material, which may be related to the characteristics and treatment of the material surface. That should be studied further. However, it is certain that the organic components of the odontogenic material were removed by calcination, eliminating the risk of immune rejection, and DNCPs can be extracted from dentin as growth factors. This study makes full use of the valuable biological resource of human extracted teeth.

The pore size of the odontogenic BCP material is equivalent to the size of the dentin tubules, which may affect the osteoconduction and osteoinduction. Therefore, in the future research, we can consider the nano-processing of the odontogenic BCP, and combine with artificial or natural biological polymers to make a porous three-dimensional scaffold loaded with DNCPs, which is believed to provide more support for the application of odontogenic biological materials. Although DNCPs are not pure, and the concentration of DNCPs above 20 $\mu\text{g}/\text{mL}$ can inhibit cell proliferation and osteogenic differentiation. In view of the animal experimental results, DNCPs and BCP alone or in combination have been shown to play a stimulative role in bone regeneration. Based on this study, we will improve the extraction method of DNCPs, and further study the *in vitro* experiment of proteins and materials promoting stem cell osteogenic differentiation.

In summary, at 4 months of implantation, the bone growth of the BCP groups was significantly increased compared with the bone growth of the β -TCP groups. A clear difference existed in degradation and bone quality between these material groups. The odontogenic BCP and DBBM have similar effects on promoting osteogenesis. DNCPs also play a significant role in new bone formation and bone matrix mineralization. Tissue-engineered bone with odontogenic growth factor and scaffolds is a promising strategy for maxillary sinus augmentation.

Supplementary Information The online version contains supplementary material available at <https://doi.org/10.1007/s13770-022-00502-z>.

Acknowledgements The authors are thankful to Center for Scientific Research and Key Lab. of Oral Diseases Research of Anhui Medical University for supporting the research. This work was supported by the Anhui Provincial Key Research and Development Plan (201904a07020062). Anhui Provincial Key Research and Development Plan, 201904a07020062, Yuanyin Wang. 2021Disciplinary Construction Project in School of Dentistry, Anhui Medical University 2021kqxkFY10.

Declarations

Conflict of interest The authors have no financial conflicts of interest.

Ethical statement The animal studies were performed after receiving approval of the Animal Research Committee of Anhui Medical University (LLSC 20210681).

References

1. Stacchi C, Rapani A, Lombardi T, Bernardello F, Nicolini V, Berton F. Does new bone formation vary in different sites within the same maxillary sinus after lateral augmentation? A prospective histomorphometric study. *Clin Oral Implants Res.* 2022;33:322–32.

2. Soardi CM, Soardi B, Wang HL. Crestal window sinus lift and Its long-term clinical outcomes. *Int J Periodontics Restorative Dent*. 2020;40:757–64.
3. Guan X, Zhang J, Chen Y, Han J, Yu M, Zhou Y. Changes in bone graft height and influencing factors after sinus floor augmentation by using the lateral window approach: a clinical retrospective study of 1 to 2 years. *J Prosthet Dent*. 2021. <https://doi.org/10.1016/j.prosdent.2021.10.010>
4. Wu Z, Meng Z, Wu Q, Zeng D, Guo Z, Yao J, et al. Biomimetic and osteogenic 3D silk fibroin composite scaffolds with nano MgO and mineralized hydroxyapatite for bone regeneration. *J Tissue Eng*. 2020;11:2041731420967791.
5. Parisi C, Salvatore L, Veschini L, Serra MP, Hobbs C, Madaghiale M, et al. Biomimetic gradient scaffold of collagen–hydroxyapatite for osteochondral regeneration. *J Tissue Eng*. 2020;11:2041731419896068.
6. Fukuba S, Okada M, Nohara K, Iwata T. Alloplastic bone substitutes for periodontal and bone regeneration in dentistry: current status and prospects. *Materials (Basel)*. 2021;14:1096.
7. Cheah CW, Al-Namnam NM, Lau MN, Lim GS, Raman R, Fairbairn P, et al. synthetic material for bone, periodontal, and dental tissue regeneration: where are we now, and where are we heading next? *Materials (Basel)*. 2021;14:6123.
8. Gao C, Wei P, Feng P, Xiao T, Shuai C, Peng S. Nano SiO₂ and MgO improve the properties of porous β -TCP scaffolds via advanced manufacturing technology. *Int J Mol Sci*. 2015;16:6818–30.
9. Wang C, Zhong D, Zhou X, Yin K, Liao Q, Kong L, et al. Preparation of a new composite combining strengthened β -tricalcium phosphate with platelet-rich plasma as a potential scaffold for the repair of bone defects. *Exp Ther Med*. 2014;8:1081–6.
10. Kato E, Lemler J, Sakurai K, Yamada M. Biodegradation property of beta-tricalcium phosphate-collagen composite in accordance with bone formation: a comparative study with Bio-Oss Collagen® in a rat critical-size defect model. *Clin Implant Dent Relat Res*. 2014;16:202–11.
11. Funayama T, Noguchi H, Kumagai H, Sato K, Yoshioka T, Yamazaki M. Unidirectional porous beta-tricalcium phosphate and hydroxyapatite artificial bone: a review of experimental evaluations and clinical applications. *J Artif Organs*. 2021;24:103–10.
12. Zhang B, Sun H, Wu L, Ma L, Xing F, Kong Q, et al. 3D printing of calcium phosphate bioceramic with tailored biodegradation rate for skull bone tissue reconstruction. *Biodes Manuf*. 2019;2:161–71.
13. Su J, Hua S, Chen A, Chen P, Yang L, Yuan X, et al. Three-dimensional printing of gyroid-structured composite bioceramic scaffolds with tuneable degradability. *Biomater Adv*. 2022;133:112595.
14. Ahn JH, Kim J, Han G, Kim D, Cheon KH, Lee H, et al. 3D-printed biodegradable composite scaffolds with significantly enhanced mechanical properties via the combination of binder jetting and capillary rise infiltration process. *Addit Manuf*. 2021;41:101988.
15. Frenken JW, Bouwman WF, Bravenboer N, Zijdeveld SA, Schulten EA, ten Bruggenkate CM. The use of Straumann Bone Ceramic in a maxillary sinus floor elevation procedure: a clinical, radiological, histological and histomorphometric evaluation with a 6-month healing period. *Clin Oral Implants Res*. 2010;21:201–8.
16. Annibaldi S, Iezzi G, Sfasciotti GL, Cristalli MP, Voza I, Mangano C, et al. Histological and histomorphometric human results of HA-Beta-TCP 30/70 compared to three different biomaterials in maxillary sinus augmentation at 6 months: a preliminary report. *Biomed Res Int*. 2015;2015:156850.
17. Bouwman WF, Bravenboer N, Ten Bruggenkate CM, Eijssackers FA, Stringa N, Schulten E. Tissue level changes after maxillary sinus floor elevation with three types of calcium phosphate ceramics: a radiological study with a 5-year follow-up. *Materials (Basel)*. 2021;14:1471.
18. Lim HC, Hong JY, Lee JS, Jung UW, Choi SH. Late-term healing in an augmented sinus with different ratios of biphasic calcium phosphate: a pilot study using a rabbit sinus model. *J Periodontal Implant Sci*. 2016;46:57–69.
19. Chai YC, Carlier A, Bolander J, Roberts SJ, Geris L, Schrooten J, et al. Current views on calcium phosphate osteogenicity and the translation into effective bone regeneration strategies. *Acta Biomater*. 2012;8:3876–87.
20. Lim HC, Kim KT, Lee JS, Jung UW, Choi SH. In vivo comparative investigation of three synthetic graft materials with varying compositions processed using different methods. *Int J Oral Maxillofac Implants*. 2015;30:1280–6.
21. Karageorgiou V, Kaplan D. Porosity of 3D biomaterial scaffolds and osteogenesis. *Biomaterials*. 2005;26:5474–91.
22. Dou W, Chen H, Chen T, Zhu Q, Jiang D, Xue Z, et al. Design and construction of a microporous CO₃²⁻-containing HA/ β -TCP biphasic ceramic as a novel bone graft material. *Mater Res Exp*. 2020;7:025401.
23. Olszta MJ, Cheng X, Jee SS, Kumar R, Kim Y-Y, Kaufman MJ, et al. Bone structure and formation: a new perspective. *Mater Sci Eng R Rep*. 2007;58:77–116.
24. Morgan S, Poundarik AA, Vashishth D. Do Non-collagenous proteins affect skeletal mechanical properties? *Calcif Tissue Int*. 2015;97:281–91.
25. Stock SR. The mineral-collagen interface in bone. *Calcif Tissue Int*. 2015;97:262–80.
26. Gorski JP. Biomineralization of bone: a fresh view of the roles of non-collagenous proteins. *Front Biosci (Landmark Ed)*. 2011;16:2598–621.
27. Bee SL, Bustami Y, Ul-Hamid A, Lim K, Abdul Hamid ZA. Synthesis of silver nanoparticle-decorated hydroxyapatite nanocomposite with combined bioactivity and antibacterial properties. *J Mater Sci Mater Med*. 2021;32:106.
28. Kim SG. Bone grafting using particulate dentin. *Key Eng Mater*. 2007;342:29–32.
29. Ravindran S, George A. Multifunctional ECM proteins in bone and teeth. *Exp Cell Res*. 2014;325:148–54.
30. Butler WT, Ritchie H. The nature and functional significance of dentin extracellular matrix proteins. *Int J Dev Biol*. 1995;39:169–79.
31. Qin C, Baba O, Butler WT. Post-translational modifications of sibling proteins and their roles in osteogenesis and dentinogenesis. *Crit Rev Oral Biol Med*. 2004;15:126–36.
32. Han S, Paeng KW, Park S, Jung UW, Cha JK, Hong J. Programmed BMP-2 release from biphasic calcium phosphates for optimal bone regeneration. *Biomaterials*. 2021;272:120785.
33. Deng N, Sun J, Li Y, Chen L, Chen C, Wu Y, et al. Experimental study of rhBMP-2 chitosan nano-sustained release carrier-loaded PLGA/nHA scaffolds to construct mandibular tissue-engineered bone. *Arch Oral Biol*. 2019;102:16–25.
34. Sun Y, Jiang Y, Liu Q, Gao T, Feng JQ, Dechow P, et al. Biomimetic engineering of nanofibrous gelatin scaffolds with non-collagenous proteins for enhanced bone regeneration. *Tissue Eng Part A*. 2013;19:1754–63.
35. Huang B, Sun Y, Maciejewska I, Qin D, Peng T, McIntyre B, et al. Distribution of SIBLING proteins in the organic and inorganic phases of rat dentin and bone. *Eur J Oral Sci*. 2008;116:104–12.
36. Zyman ZZ, Tkachenko MV, Polevodin DV. Preparation and characterization of biphasic calcium phosphate ceramics of desired composition. *J Mater Sci Mater Med*. 2008;19:2819–25.

37. Brown O, McAfee M, Clarke S, Buchanan F. Sintering of biphasic calcium phosphates. *J Mater Sci Mater Med*. 2010;21:2271–9.
38. Collins MO, Yu L, Choudhary JS. Analysis of protein phosphorylation on a proteome-scale. *Proteomics*. 2007;7:2751–68.
39. Yang XJ. Multisite protein modification and intramolecular signaling. *Oncogene*. 2005;24:1653–62.
40. Kim JS, Cha JK, Lee JS, Choi SH, Cho KS. Increased osteoinductivity and mineralization by minimal concentration of bone morphogenetic protein-2 loaded onto biphasic calcium phosphate in a rabbit sinus. *J Periodontal Implant Sci*. 2016;46:350–9.
41. Zhang W, Wang X, Wang S, Zhao J, Xu L, Zhu C, et al. The use of injectable sonication-induced silk hydrogel for VEGF(165) and BMP-2 delivery for elevation of the maxillary sinus floor. *Biomaterials*. 2011;32:9415–24.
42. Del Fabbro M, Bortolin M, Taschieri S, Weinstein RL. Effect of autologous growth factors in maxillary sinus augmentation: a systematic review. *Clin Implant Dent Relat Res*. 2013;15:205–16.
43. Khouly I, Pardiñas López S, Aliaga I, Froum SJ. Long-term implant survival after 100 maxillary sinus augmentations using plasma rich in growth factors. *Implant Dent*. 2017;26:199–208.
44. Dimitriou R, Tsiridis E, Giannoudis PV. Current concepts of molecular aspects of bone healing. *Injury*. 2005;36:1392–404.
45. Lee CP, Colombo JS, Ayre WN, Sloan AJ, Waddington RJ. Elucidating the cellular actions of demineralised dentine matrix extract on a clonal dental pulp stem cell population in orchestrating dental tissue repair. *J Tissue Eng*. 2015;6:2041731415586318.
46. Walsh DP, Raftery RM, Chen G, Heise A, O'Brien FJ, Cryan SA. Rapid healing of a critical-sized bone defect using a collagen-hydroxyapatite scaffold to facilitate low dose, combinatorial growth factor delivery. *J Tissue Eng Regen Med*. 2019;13:1843–53.
47. Chen FM, Zhang M, Wu ZF. Toward delivery of multiple growth factors in tissue engineering. *Biomaterials*. 2010;31:6279–308.
48. Kavukcuoglu NB, Denhardt DT, Guzelsu N, Mann AB. Osteopontin deficiency and aging on nanomechanics of mouse bone. *J Biomed Mater Res A*. 2007;83:136–44.
49. Hansma PK, Fantner GE, Kindt JH, Thurner PJ, Schitter G, Turner PJ, et al. Sacrificial bonds in the interfibrillar matrix of bone. *J Musculoskelet Neuronal Interact*. 2005;5:313–5.
50. Nikel O, Laurencin D, McCallum SA, Gundberg CM, Vashishth D. NMR investigation of the role of osteocalcin and osteopontin at the organic-inorganic interface in bone. *Langmuir*. 2013;29:13873–82.
51. Poundarik AA, Diab T, Sroga GE, Ural A, Boskey AL, Gundberg CM, et al. Dilatational band formation in bone. *Proc Natl Acad Sci U S A*. 2012;109:19178–83.
52. Wang K, Leng Y, Lu X, Ren F. Calcium phosphate bioceramics induce mineralization modulated by proteins. *Mater Sci Eng C Mater Biol Appl*. 2013;33:3245–55.
53. Wang J, Chen Y, Zhu X, Yuan T, Tan Y, Fan Y, et al. Effect of phase composition on protein adsorption and osteoinduction of porous calcium phosphate ceramics in mice. *J Biomed Mater Res A*. 2014;102:4234–43.
54. LeGeros RZ, Lin S, Rohanizadeh R, Mijares D, LeGeros JP. Biphasic calcium phosphate (BCP) Bioceramics: preparation, properties and applications. *J Mater Sci Mater Med*. 2003;14:201–9.
55. Rh Owen G, Dard M, Larjava H. Hydroxyapatite/beta-tricalcium phosphate biphasic ceramics as regenerative material for the repair of complex bone defects. *J Biomed Mater Res B Appl Biomater*. 2018;106:2493–512.
56. Jones AC, Arns CH, Huttmacher DW, Milthorpe BK, Sheppard AP, Knackstedt MA. The correlation of pore morphology, interconnectivity and physical properties of 3D ceramic scaffolds with bone ingrowth. *Biomaterials*. 2009;30:1440–51.
57. Zhu XD, Fan HS, Xiao YM, Li DX, Zhang HJ, Luxbacher T, et al. Effect of surface structure on protein adsorption to biphasic calcium-phosphate ceramics in vitro and in vivo. *Acta Biomater*. 2009;5:1311–8.
58. Khan MUA, Abd Razak SI, Mehboob H, Abdul Kadir MR, Anand TJS, Inam F, et al. Synthesis and characterization of silver-coated polymeric scaffolds for bone tissue engineering: antibacterial and in vitro evaluation of cytotoxicity and biocompatibility. *ACS Omega*. 2021;6:4335–46.

Publisher's Note Springer Nature remains neutral with regard to jurisdictional claims in published maps and institutional affiliations.

Springer Nature or its licensor (e.g. a society or other partner) holds exclusive rights to this article under a publishing agreement with the author(s) or other rightsholder(s); author self-archiving of the accepted manuscript version of this article is solely governed by the terms of such publishing agreement and applicable law.